4.1 Introduction

The energy from biomass can be extracted through biological (enzymatic digestion and fermentation), and thermochemical (torrefaction, liquefaction, pyrolysis, gasification etc.) conversion routes; however later has gained dominance due to its fast and efficient nature (Dacres et al., 2019). The torrefied biomass exhibits improved characteristics than raw biomass in terms of less moisture content, higher HHV, lower H/C and O/C ratio. Torrefaction also improves the grindability and lowers the water sorption characteristics of biomass (Bach et al., 2017a; Bach et al., 2017b; Chen et al., 2016b; Ren et al., 2013a). Eventually, there are two ways through which energy can be extracted from the torrefied biomass viz. either direct use of treated biomass in pyrolysis and gasification or co-pyrolysis, co-gasification with other biomass, plastic and municipal waste. Besides, these days blending of torrefied biomass with coal in thermal power plants are common practice (Bada et al., 2014; Kastanaki et al., 2002; Moghtaderi et al., 2004; Pan et al., 2000; Vuthaluru, 2004; Zhang et al., 2007).

So, in order to explore the torrefied biomass and to achieve the best utilization for bio-energy generation, kinetic and thermodynamic parameters along with model prediction of reaction mechanism become essential. The recommendations suggested by the kinetic committee of the International Confederation for Thermal Analysis and Calorimetry (ICTAC), the thermogravimetric analysis (TGA) is one of the most prevalent and effective methods to describe the thermal decomposition behavior and kinetics of biomass and coal conversion (Vyazovkin et al., 2011). Through TGA and DTG data, kinetic parameters such as activation energy and pre-exponential factor can be investigated. Furthermore, the thermodynamic parameters may also be interpreted based on the kinetic parameters.

The kinetic parameters (activation energy, pre-exponential factor), thermodynamic parameters (enthalpy, Gibbs free energy, and entropy) and reaction mechanism are very important for design, optimization, and scaling of process reactor and parameters (Hu et al., 2018). The behavior of torrefied biomass towards thermochemical conversion might be different from raw biomass. Also, during blending of torrefied biomass with coal in thermal power plant, the process will be affected by the distinctive kinetic, thermodynamic parameters and reaction mechanism followed individually by torrefied biomass and coal. So, the deep in-sight about the kinetic, thermodynamic parameter as well as reaction mechanism of torrefied biomass is required.

4.2 Materials and methods

4.2.1 Material collection, preparation, and characterization

The detailed discussion about material collection, preparation and characterization such as proximate and ultimate analysis has been discussed in Chapter 3. The proximate, ultimate, HHV and other parameters are presented in Table 3.1 of Chapter 3 and the relevant discussion is carried out in subsequent sections. The hemicellulose, cellulose, and lignin components of biomass were determined following the protocol mentioned by Bledzki et al. (Bledzki et al., 2010). Extractive component was calculated by difference.

4.2.2 Experimental procedure for torrefaction and pyrolysis of torrefied biomass

The torrefaction of biomass was carried out in a laboratory fixed bed reactor at 220, 250, and 280 ℃ with a retention time of 40 min, and a heating rate of 15 ℃/min. The schematic

diagram of the experimental setup, detailed procedure has been discussed in Chapter 3. The thermogravimetric analyzer (NETZSCH TG 209F1 Libra) was used to carry out pyrolysis of DAN, TAN220, TAN250, TAN280 at three different heating rates 5, 10, 15 K/min, between the temperature ranges from 298 to 1073 K. Nitrogen gas (99.99%, purity), at a flow rate of 20 mL/min was used as a carrier. 5 mg of each biomass sample was taken. In each experiment, initially, nitrogen gas was purged into the TGA for 20 min at an initial temperature to avoid undesirable oxidation of sample during pyrolysis. The sample was kept for 20 min at 1073 K when the experiment was over.

4.2.3 Kinetic study

The chemical composition and physical characteristics vary from one biomass to another. Consequently, pyrolysis becomes a complex process and various biomass shows different behavior (Huang et al., 2016; Sriram & Swaminathan, 2018). The TGA and DTG data were used to obtain the kinetic and thermodynamic parameters for thermal degradation of DAN and TAN during pyrolysis. The general pyrolysis reaction can be represented as (Kaur et al., 2018; Slopiecka et al., 2012):

$$\text{Biomass} \xrightarrow{k} \text{Bio-char} + \text{volatile}$$

A general expression for non-isothermal kinetics for solid decomposition can be expressed as follows:

$$\frac{d\alpha}{dt} = k\,(T)\,f\,(\alpha) \qquad (4.1)$$

where, k is the rate constant, and α is the fractional conversion during thermal decomposition of solid biomass. Biomass conversion can be defined as follows:

$$\alpha = \frac{m_0 - m_t}{m_0 - m_f} \quad (4.2)$$

where, m_0 is the initial mass of the sample, m_t is the mass of sample at any time t, and m_f is the final mass of the sample.

The rate constant is a function of temperature and may be expressed as follows:

$$k\,(T) = Ae^{-E_a/RT} \quad (4.3)$$

where E_a is activation energy, A is pre-exponential factor and R is universal gas constant.

Combining Eqs. (4.1) and (4.3) gives the fundamental expression (4.4) for the analytical method to calculate kinetic parameters, on the basis of TGA data.

$$\frac{d\alpha}{dt} = Ae^{-E_a/RT}\, f\,(\alpha) \quad (4.4)$$

The TGA analysis was carried out at a constant heating rate given as:

$$\beta = \frac{dT}{dt} \quad (4.5)$$

The conversion can be expressed as the function of temperature. However, the temperature is dependent on the heating rate also. Therefore,

$$\frac{d\alpha}{dT} = \frac{d\alpha}{dt}\frac{dt}{dT} \quad (4.6)$$

$$\frac{d\alpha}{dT} = \frac{d\alpha}{dt}\frac{1}{\beta} \quad (4.7)$$

Combining Eqs. (4.4) and (4.7)

$$\frac{d\alpha}{dT} = \frac{A}{\beta}\, e^{-E_a/RT}\, f\,(\alpha) \quad (4.8)$$

Integrating both sides of Eqs. (4.8) gives:

$$g(\alpha) = \int_0^{\alpha} \frac{d\alpha}{f(\alpha)} = \frac{A}{\beta} \int_0^{T} e^{-E_a/RT} dT \quad (4.9)$$

where, $g(\alpha)$ is the integral function of conversion α. The kinetic model $f(\alpha)$ is an algebraic expression related with a physical model which describes the kinetics of the solid state reaction. Functional forms of $f(\alpha)$ and $g(\alpha)$ representing different reaction mechanism are listed in Table 4.1. These expressions can be used to predict the reaction mechanism, reflected by the dynamic TGA curves. In the present study, the activation energy was obtained from non-isothermal TGA. The methods used to determine the kinetic parameters are isoconversional or model free methods. The kinetic parameters were estimated from numerous plots at different heating rates at same level of conversion.

4.2.4 Model-free isoconversional methods

The thermal decomposition of biomass is very complex process and it is characterized by multiple reactions with different rates. Thus, simple kinetic model cannot be applicable for such reactions. To investigate the in-depth analysis of thermal decomposition of biomass, isoconversional models are frequently used. The isoconversional models used in present work are: (1) Kissinger-Akahira-Sunose (KAS) method, (2) Ozawa-Wall- Flynn (OWF) method, (3) Friedman method, and (4) Starink method.

4.2.4.1. The Kissinger-Akahira-Sunose (KAS) method

KAS method predicted the relationship between heating rate and activation energy through non-isothermal linear integral as per the Eqs. (4.10)

$$\ln\left(\frac{\beta}{T_\alpha{}^2}\right) = \ln\left(\frac{AR}{E_\alpha g(\alpha)}\right) - \frac{E_\alpha}{RT_\alpha} \quad (4.10)$$

where T_α is the temperature at conversion α. The plot between $\ln\left(\frac{\beta}{T_\alpha{}^2}\right)$ and $\frac{1}{T_\alpha}$, at a constant value of conversion gives a straight line, whose slope can be used to calculate activation energy.

4.2.4.2 The Ozawa-Wall- Flynn (OWF) method

OWF method can be derived by integrating Eqs. (4.11), and then Doyle's approximation was implied over temperature integral. The resulting equations are obtained as Eqs. (4.12) and (4.13). At every conversion three points for $\ln\beta$ and $\frac{1}{T_\alpha}$ can be obtained at three heating rates. The plot between these points will give a straight line having slope $(-1.052\frac{E_a}{R})$ which can be used to compute activation energy.

$$\frac{d\alpha}{dT} = \frac{A}{\beta} e^{-E_a/RT} f(\alpha) \quad (4.11)$$

$$\ln\beta = \ln\left(\frac{AE_\alpha}{Rg(\alpha)}\right) - 5.3305 - 1.052\frac{E_\alpha}{RT_\alpha} \quad (4.12)$$

or

$$\ln\beta = \ln\left(\frac{0.0048AE_\alpha}{Rg(\alpha)}\right) - 1.052\frac{E_\alpha}{RT_\alpha} \quad (4.13)$$

4.2.4.3. Friedman method

The Friedman equation can be derived by rearranging Eqs. (4.14) and then taking natural logarithm on both sides, Eqs. (4.15) and (4.16) can be deduced.

$$\frac{d\alpha}{dT} = \frac{A}{\beta} e^{-E_a/RT} f(\alpha) \quad (4.14)$$

$$\beta \frac{d\alpha}{dT} = \text{A } e^{-E_a/RT_\alpha} f(\alpha) \quad (4.15)$$

$$\ln\left(\beta \frac{d\alpha}{dT}\right) = \ln [A\ f\ (\alpha)]\ - \frac{E_\alpha}{RT_\alpha} \quad (4.16)$$

The plot between $\ln\left(\beta \frac{d\alpha}{dT}\right)$ and $\frac{1}{T_\alpha}$ will give a straight line having slope, $(-\frac{E_\alpha}{R})$ which can be used to compute activation energy.

4.2.4.4. Starink method

Starink analyzed the KAS and OWF methods to get the following equation.

$$\ln\left(\frac{\beta}{T_\alpha{}^S}\right) = \text{C} - \frac{BE_\alpha}{RT_\alpha} \quad (4.16)$$

where, S and B take different values. By using temperature integral approximation, Starink obtained the value of S and B as 1.92, and 1.0008 respectively. Then Eqs. (4.16) can be rewritten as:

$$\ln\left(\frac{\beta}{T^{1.92}}\right) = \text{C} - 1.0008\ \frac{E_\alpha}{RT_\alpha} \quad (4.17)$$

At every conversion, three points for $\ln\left(\frac{\beta}{T^S}\right)$ and $\frac{1}{T_\alpha}$ can be obtained at three heating rates. The plot between these points will give a straight line having slope, $(-1.0008\frac{E_\alpha}{R})$ which can be used to compute activation energy.

4.2.5 Prediction of reaction model

The model for solid state reaction during pyrolysis of biomass is investigated by Z-master plot associated with Criado method (Eqs. 4.18) (Criado, 1978). Master plots are the plots which depend on the reaction kinetic model however they are independent of kinetic parameters like activation energy and pre-exponential factor (Dhyani et al., 2017).

$$\frac{Z(\alpha)}{Z(0.5)} = \frac{f(\alpha)\times g(\alpha)}{f(0.5)\times g(0.5)} = \left(\frac{T_\alpha}{T_{0.5}}\right)^2 \times \frac{(d\alpha/dT)_\alpha}{(d\alpha/dT)_{0.5}} \quad (4.18)$$

The above Equation is employed to generate the master plots equivalent to various solid-state reaction mechanism as mentioned in Table 4.1. In this Equation, the term [$f(\alpha) \times g(\alpha)/f(0.5)\times g(0.5)$] will give a theoretical curve, which signifies the characteristics of each reaction mechanism. While, the term [$(T_\alpha/T_{0.5})^2 \times ((d\alpha/dT)_\alpha/(d\alpha/dT)_{0.5})$] will reduce to a curve obtained from experimental values. The conversion value α = 0.5 is selected as a reference value, at which, master plot from all the reaction mechanism and experimental curve will intersect to each other at the value of $[Z(\alpha)/Z(0.5)]$ = 1. The principal reaction mechanism for experimental value is decided by comparing the theoretical and experimental curves. The theoretical curve which is closest to the experimental curve is selected as reaction mechanism (Dhyani et al., 2017; Mishra et al., 2015; Poletto et al., 2012).

Table 4.1 Models of pyrolysis reaction with different values of $f(\alpha)$ and g (α)

Solid state process	**Mechanism**	$f(\alpha)$	$g(\alpha)$
One dimensional diffusion	D1	$1/(2\alpha)$	α^2
Two-dimensional diffusion (Valensi model)	D2	$[-\ln(1-\alpha)]^{-1}$	$(1-\alpha)\ln(1-\alpha)+\alpha$
Three-dimensional diffusion (Jander model model)	D3	$\frac{3}{2}(1-\alpha)^{2/3}\,[1-(1-\alpha)^{1/3}]^{-1}$	$[1-(1-\alpha)^{1/3}]^2$
Three-dimensional diffusion (Ginstlinge-Brounshtein model)	D4	$\frac{3}{2}[(1-\alpha)^{1/3}-1]^{-1}$	$1-\frac{2}{3}\alpha-(1-\alpha)^{2/3}$
Contracting cylinder	F2	$2(1-\alpha)^{1/3}$	$1-(1-\alpha)^{1/2}$
Contracting sphere	F3	$(1-\alpha)^{2/3}$	$1-(1-\alpha)^{1/3}$
Power law	P2/3	$\frac{2}{3}\alpha^{-1/2}$	$\alpha^{3/2}$
Power law	P2	$2\alpha^{1/2}$	$\alpha^{1/2}$
Power law	P3	$3\alpha^{2/3}$	$\alpha^{1/3}$
Power law	P4	$4\alpha^{3/4}$	$\alpha^{1/4}$
Avrami-Erofeev	A1	$\frac{1}{2}(1-\alpha)\,[-\ln(1-\alpha)]^{1/3}$	$[-\ln(1-\alpha)]^{2/3}$
Avrami-Erofeev	A2	$2(1-\alpha)\,[-\ln(1-\alpha)]^{1/2}$	$[-\ln(1-\alpha)]^{1/2}$
Avrami-Erofeev	A3	$3(1-\alpha)\,[-\ln(1-\alpha)]^{2/3}$	$[-\ln(1-\alpha)]^{1/3}$
Avrami-Erofeev	A4	$4(1-\alpha)\,[-\ln(1-\alpha)]^{3/4}$	$[-\ln(1-\alpha)]^{1/4}$
1st order random nucleation having one nucleus on individual particle	R1	$(1-\alpha)$	$-\ln(1-\alpha)$
2nd order random nucleation having two nucleus on individual particle	R2	$(1-\alpha)^2$	$(1-\alpha)^{-1}-1$
3rd order random nucleation having three nucleus on individual particle	R3	$(1-\alpha)^3$	$\frac{1}{2}[(1-\alpha)^{-2}-1]$

4.2.6 Estimation of pre-exponential factor and thermodynamic parameter

Using isoconversional methods discussed earlier in section 2.5, activation energy was calculated at different level of conversion; however, the pre-exponential factor and reaction mechanism given by isoconversional method is not reliable (Dhyani et al., 2017). For pre-exponential factor Kissinger's method was used given by Eqs. (4.19). Kissinger's method is employed at different heating rate; however it gives only a single value of activation energy for overall conversion process. Thus it was not used to calculate activation energy in this study. Once, the activation energy is known at different value of conversion, Eqs. (4.20) can be used to calculate pre-exponential factor. In this study, activation energy obtained from KAS method was used to calculate pre-exponential factor.

$$\ln\left(\frac{\beta}{{T_p}^2}\right) = \ln\left(\frac{AR}{E}\right) - \frac{E}{RT_p} \tag{4.19}$$

$$A=\beta . E_\alpha .\text{Exp}\left(\frac{E_\alpha}{RT_p}\right)/(R.{T_p}^2) \tag{4.20}$$

Once the activation energy and pre-exponential factor was known at different level of conversion, the thermodynamic parameters such as change in enthalpy (ΔH), change in Gibbs free energy (ΔG), and change in entropy (ΔS) were calculated using the equation (4.21)-(4.23).

$$\Delta H = E_\alpha - RT_\alpha \tag{4.21}$$

$$\Delta G = E_\alpha + R.\, T_p .\ln\left(\frac{K_B.T_m}{h.A}\right) \tag{4.22}$$

$$\Delta S = \frac{\Delta H - \Delta G}{T_p} \tag{4.23}$$

where, K_B is the Boltzmann constant (1.381*10 $^{-23}$ J/K), h is the Plank constant (6.626 *10 $^{-23}$ J.s), and T_p, is the peak temperature in the DTG curve.

4.3 Results and discussion

4.3.1. Yield of product and physicochemical characteristics of DAN and torrefied biomass

Table 4.2 represents the yield of solid product at 220, 250, and 280 ℃ with a constant retention time of 40 min and a heating rate of 15 ℃/min. The detailed discussion about product yield and physicochemical characteristics of DAN and TAN has been discussed in Chapter 3. Table 4.2 represents the fiber analysis of DAN and TAN. The hemicellulose, cellulose, lignin, and extractives present in DAN are 28.51, 41.66, 23.90, and 5.95%, respectively. The hemicellulose and extractives content decreased while the lignin content increased with increasing temperature during torrefaction. On the other hand, the cellulose content increased at lower temperature (TAN-220) and then goes on decreasing on further increase in temperature. Hemicellulose, cellulose, and extractives decreased by 69.34, 21.84, and 53.61%, respectively. Though, lignin content increased by 57.27%. Hence, it was noted that, in the course of torrefaction, the decomposition of hemicellulose is more pronounced than the decomposition of cellulose and lignin.

Table 4.2 Fiber analysis of DAN and torrefied biomass and solid yield during torrefaction

Analysis	**DAN**	**TAN-220**	**TAN-250**	**TAN-280**
Fiber analysis(wt %, dry basis)				
Hemicellulose	28.64±0.95	25.49±0.77	17.38±0.56	10.52±1.52
Cellulose	41.66±0.90	44.51±1.89	38.38±1.04	33.61±0.82
Lignin	24.20±0.43	27.71±1.49	41.25±1.24	54.24±1.41
Extractive*	5.50±0.48	2.29±0.23	2.99±0.24	1.63±0.26
Solid yield (wt%)	-	71.28	57.09	42.71

* calculated by difference

4.3.2 Thermogravimetric analysis

The pyrolysis behavior of DAN, TAN-220, TAN-250, and TAN-280 at a heating rate of 5, 10, and 15 K/min is shown in Figs 4.1 (a-d) and Figs 4.2 (a-d). The whole degradation process can be categorized into three major stages: (1) drying, (2) devolatilization, and (3) char formation. The first stage is accompanied with the elimination of surface moisture and some light volatile compounds (Saikia et al., 2018), and it was noticed that mass loss owing to moisture for torrefied biomass (TAN-220, TAN-250, and TAN-280) is slightly lesser than the DAN. The second stage is associated with the devolatilization process which was accompanied by major mass loss from biomass due to degradation of the major portion of hemicellulose and cellulose. At, the third stage, lignin decomposition is more pronounced. The TGA curve in this zone has a flat and long tail. Accordingly, the mass loss in this stage is lower than the second stage. Considering a fixed amount of mass loss for example 10%, for DAN and torrefied biomass (TAN-220, TAN-250, and TAN-280), at a heating rate of 5 K/min, it was attained at 520, 572, 586, and 610 K, respectively. It shows that

decomposition shifted to a higher temperature in case of TAN and extent of the shift in temperature increases with increase in temperature during torrefaction. The decomposition of hemicellulose and cellulose takes place between 200-350 ℃, whereas; lignin decomposes in a wider range of temperature between 280-600 ℃ (Ren et al., 2013a; Yang et al., 2007). It was noticed from Table 4.2 that major fraction of hemicellulose degraded along with limited degradation of cellulose during torrefaction. This may be the reason for shifting of onset devolatilization temperature in case of TAN. Additionally, inconsistency in thermal degradation of biomass component is also responsible for deviation in residual char yield. The residual char yield after pyrolysis of DAN and torrefied biomass (TAN-220, TAN-250, and TAN-280) at a heating rate of 5 K/min, was observed to be 17.09, 27.76, 49.30, and 66.72%, respectively. In addition, slight variation in residual char yield was also observed due to the variation of heating rate. The higher residual char yield in case of TAN may be due to large mass loss through decomposition of hemicellulose and lignin and also due to the cross-linkage reaction during the pyrolysis of TAN (Park et al., 2013; Ren et al., 2013a; Wannapeera et al., 2011a). Thus, it may be mentioned that higher the torrefaction temperature, higher will be the char yield during pyrolysis.

Figs. 4.2 (a-d) present the DTG curve of DAN and torrefied biomass (TAN-220, TAN-250, and TAN-280). In DTG curve, the presence of shoulder on the left side of the plot describes the degradation of hemicellulose in the biomass and is typically noted at around 573 K (Müller-Hagedorn et al., 2003; Yang et al., 2007). In case of DAN, similar shoulders appear at 548, 563, and 573 K at a heating rate of 5, 10, and 15 K/min, respectively, as shown in Fig. 4.2 (a). On the other hand, the similar shoulder disappeared in case of torrefied biomass (TAN-220, TAN-250, and TAN-280) (Figs.4.2 (b-d)), suggesting that

major fraction of hemicellulose has already being degraded in the course of torrefaction. Yang et al. (Yang et al., 2007) reported that peaks appeared in the DTG curve with maximum weight loss signifies the occurrence of cellulose in the biomass. The temperature noted at the peaks in DTG curve for DAN was 623, 639, and 642 K at a heating rate of 5, 10, and 15 K/min, respectively, as shown in Fig.4.2 (a). For torrefied biomass (TAN-220) the cellulose peak temperature was noted at 622, 634, and 639 K, at a heating rate of 5, 10, and 15 K/min, respectively (Fig. 4.2 (b)). However, in case of torrefied biomass (TAN-250), peak temperature was noted at 611, 623, and 623 K, at a heating rate of 5, 10, and 15 K/min, respectively. In addition, another peak to the right side of the cellulose peak can be observed at 677, 688, and 695 K, at a heating rate of 5, 10, and 15 K/min, respectively (Fig.4.2 (c)). The appearance of second peak may be attributed to the degradation of lignin. Conversely, in case of torrefied biomass (TAN-280), in place of hemicellulose and cellulose peak, a broader peak at 769, 783, and 798 K, at a heating rate of 5, 10, and 15 K/min, respectively, were observed (Fig.4.2 (d)). These broader peaks are associated with the degradation of lignin. Similar results were also observed by Tong et al. (Tong et al., 2018) Furthermore, comparing the peak intensity of DAN and torrefied biomass (TAN-220, TAN-250, and TAN-280) at particular heating rate say 5 K/min, it was found to be 5.12, 6.11, 1.49 and 0.41 wt%/min, respectively. The increase in peak intensity of TAN-220 (Fig.4.2 (b)) than the DAN may be due to higher amount of relative cellulose content in TAN-220 than the DAN as presented in Table 4.2. On further increase in temperature, there was decrease in peak intensity.

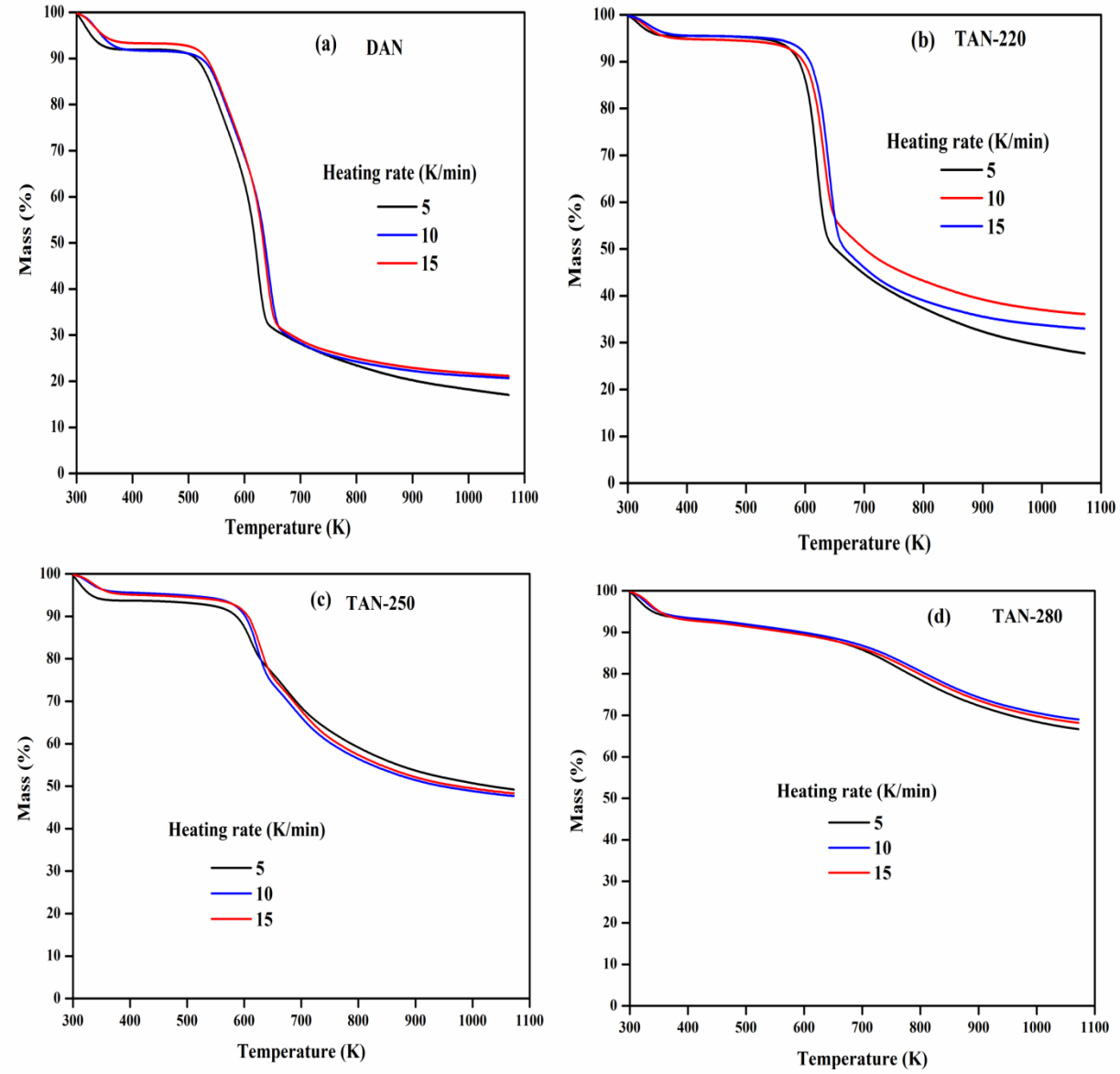

Figure 4.1 TGA analysis of DAN and torrefied biomass at different heating rate: (a) DAN (b) TAN-220 (c) TAN-250, and (d) TAN-280.

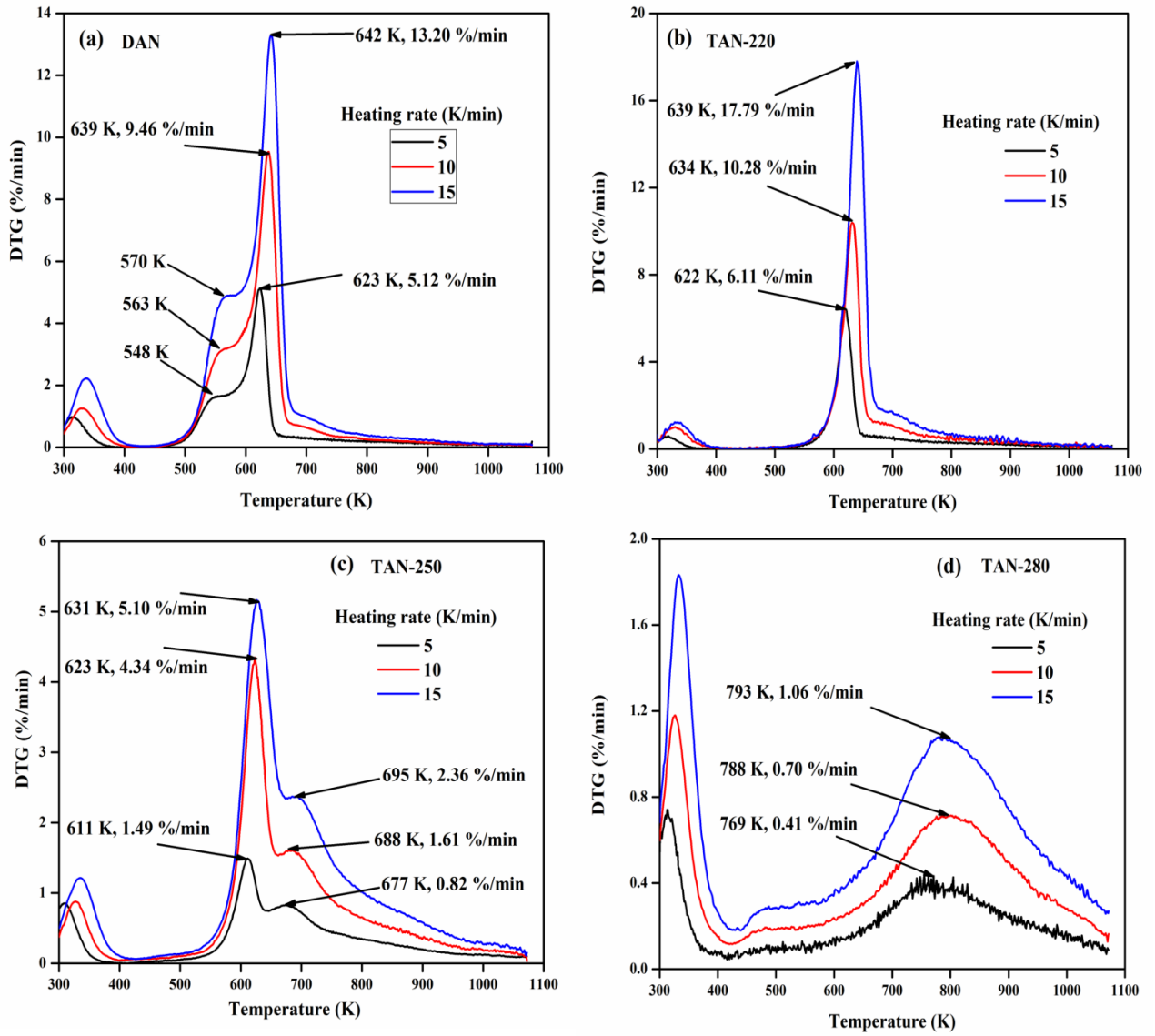

Figure 4.2 DTG analysis of DAN and torrefied biomass at different heating rate: (a) DAN (b) TAN-220 (c) TAN-250, and (d) TAN-280.

4.3.3 Kinetic analysis

The estimation of the kinetic parameters is very useful for efficient design and scaling of process reactors at industrial level (Kaur et al., 2018). The decomposition kinetic analysis of DAN and torrefied biomass (TAN-220, TAN-250, and TAN-280) was performed by applying four isoconversional methods such as KAS, OWF, Friedman and Starink at different degree of conversion ranging from 0.1 to 0.9. The isoconversional plots obtained from four methods for DAN and torrefied biomass (TAN-220, TAN-250, and TAN-280) are shown in Figs. 4.3, 4.4, 4.5 and 4.6. It can be seen that, with an increase in conversion, the slope of isoconversional lines are also changing. The slopes of these lines are used to obtain the activation energy. Thus, the value of activation energy also changes accordingly as presented in Table 4.3. The variation of activation energy with the degree of conversion is shown in Fig. 4.7. The activation energy obtained from KAS, Friedman, and Starink methods for DAN and torrefied biomass (TAN-220, TAN-250, and TAN-280) are comparable. However, slightly higher activation energy was noticed in case of OWF method as depicted by Table 4.3. The difference in activation energy from different method may be due to the assumptions and approximation adopted by different methods (Kaur et al., 2018). For example, in case of OWF method, for integral term $\int_0^T \exp\left(\frac{-E}{RT}\right) dT$, the analytical solution is not possible. Thus, Doyle's approximation was used, though Friedman method does not adopt any such approximation (Doyle, 1962; Yuan et al., 2017). The value of activation energy changes with conversion during the pyrolysis, illustrating the multi-stage kinetics rather than single stage and complexity of process during biomass conversion through pyrolysis. Therefore, the overall decomposition of biomass is

established by a multi-stage reaction mechanism where every single stage added partially to global mechanism depending upon the extent of decomposition.

The activation energy is the minimum amount of energy required to proceed a reaction. Thus, higher activation energy hinders the start of a reaction. Activation energy is also useful in deciding the reactivity of fuel (Kaur et al., 2018). The activation energy of DAN and torrefied biomass (TAN-220, TAN-250, and TAN-280) was calculated using KAS, OWF, Friedman and Starink methods as discussed in section 2.5. For DAN, the calculated value of activation energy from these methods varied within 211.49-221.58 kJ/mol. The activation energy for decomposition of torrefied biomass (TAN-220, TAN-250, and TAN-280) varied within 241.58-261.83, 185.06-198.89, and 121.83-132.98 kJ/mol, respectively. The activation energy of component of biomass (hemicellulose, cellulose and, and lignin) are different. Vamvuka et al. (Vamvuka et al., 2003) reported the activation energy of cellulose, hemicellulose, and lignin in the range of 145-285, 90-125 and 30-39 kJ/mol individually. The highest activation energy was reported for cellulose, followed by hemicellulose and then lignin. Thus the biomass having higher amount of cellulose will have higher activation energy. The relative amount of cellulose in TAN-220 is higher than the DAN as presented in Table 4.2. Accordingly, higher activation energy in case of TAN-220 than the DAN was noticed. On further increasing the temperature during torrefaction, the degradation of cellulose also becomes significant. Thus activation energy of TAN-250 and TAN-280 are lower than DAN. The lower activation energy of TAN-280 makes it suitable for thermochemical conversion. In addition, it can be used in co-firing with other biomass or coal etc.

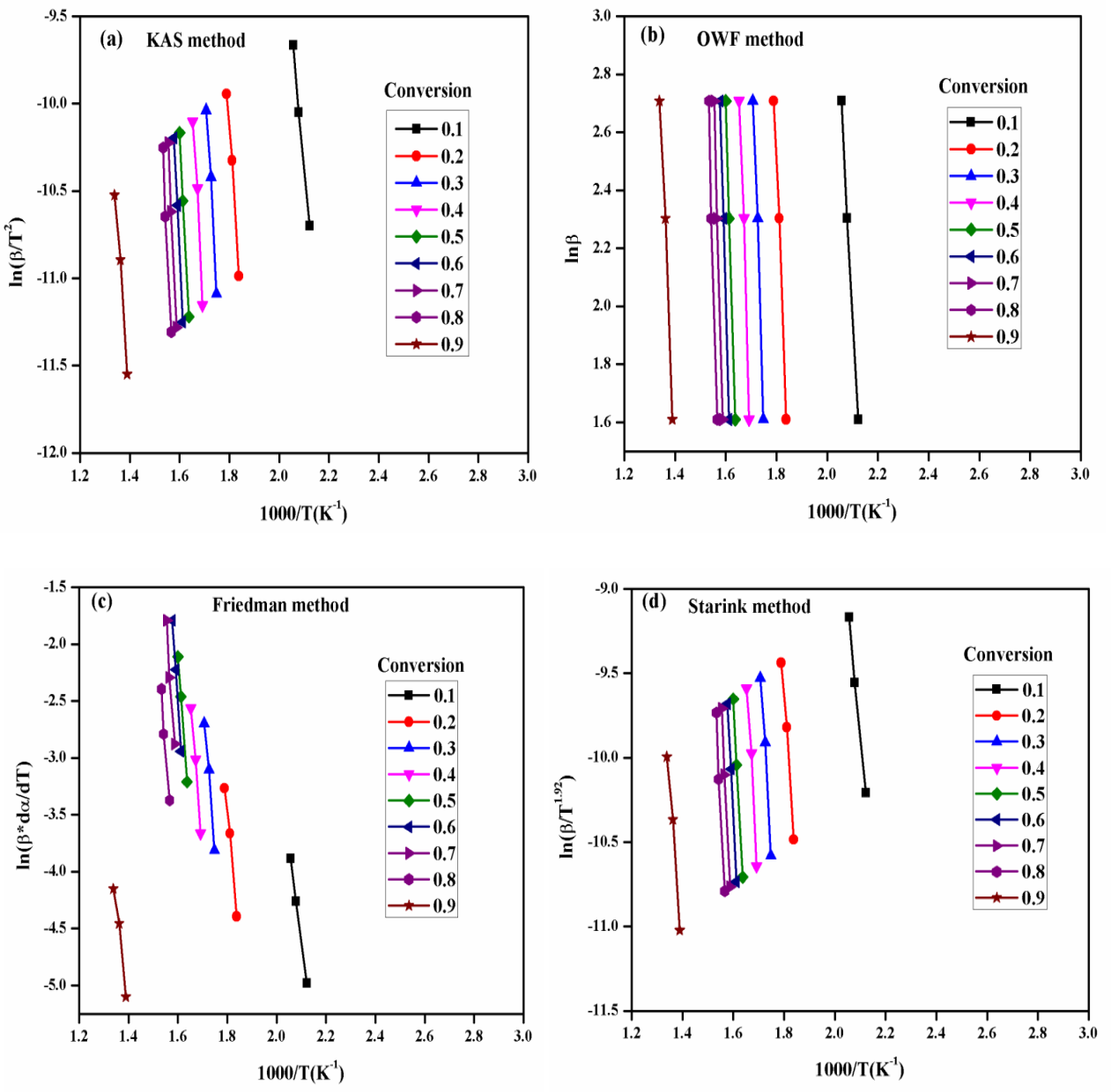

Figure 4.3 Kinetic plots for DAN using (a) KAS, (b) OWF, (c) Friedman, and (d) Starink models.

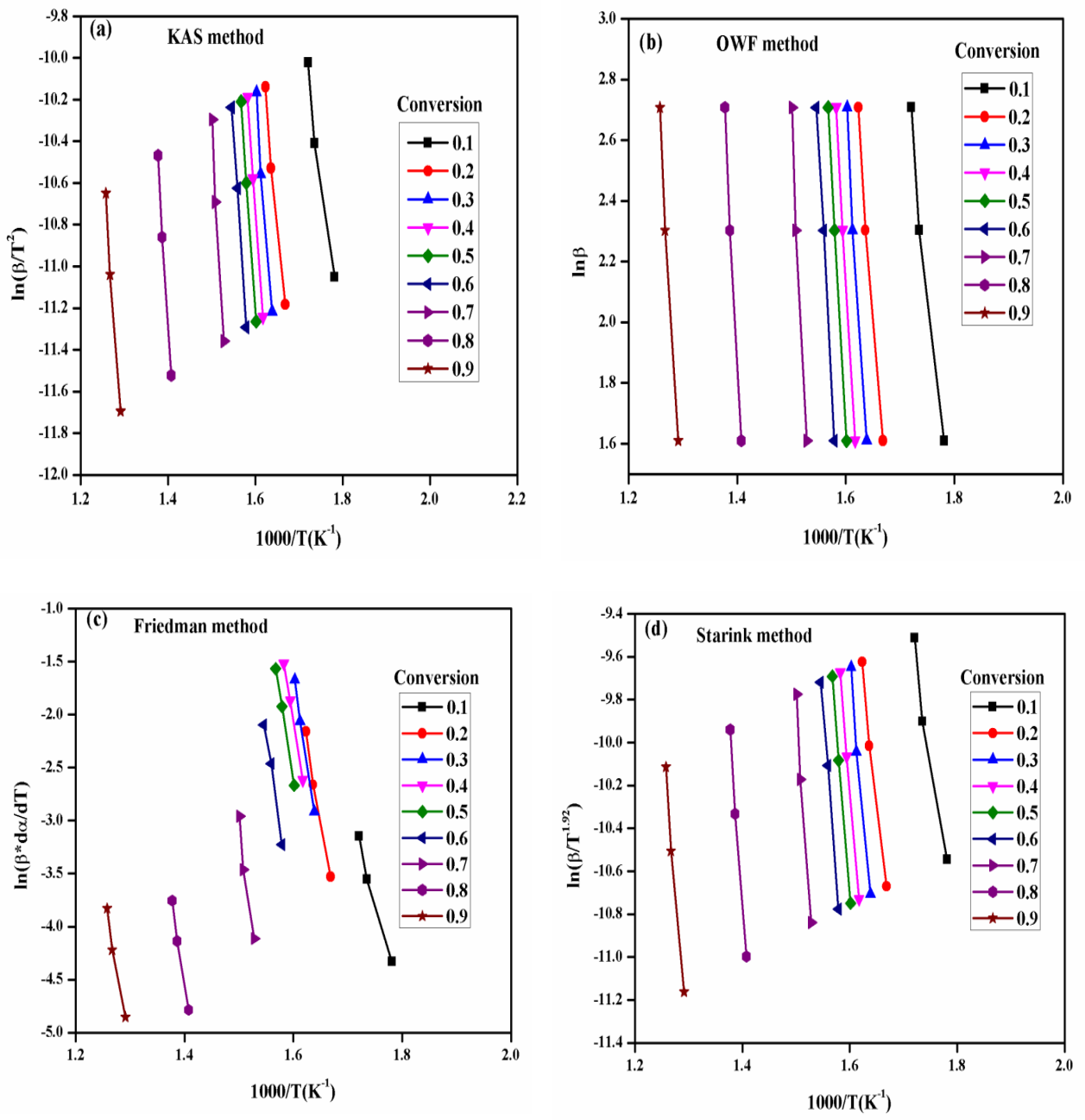

Figure 4.4 Kinetic plots for TAN-220 using (a) KAS, (b) OWF, (c) Friedman, and (d) Starink models.

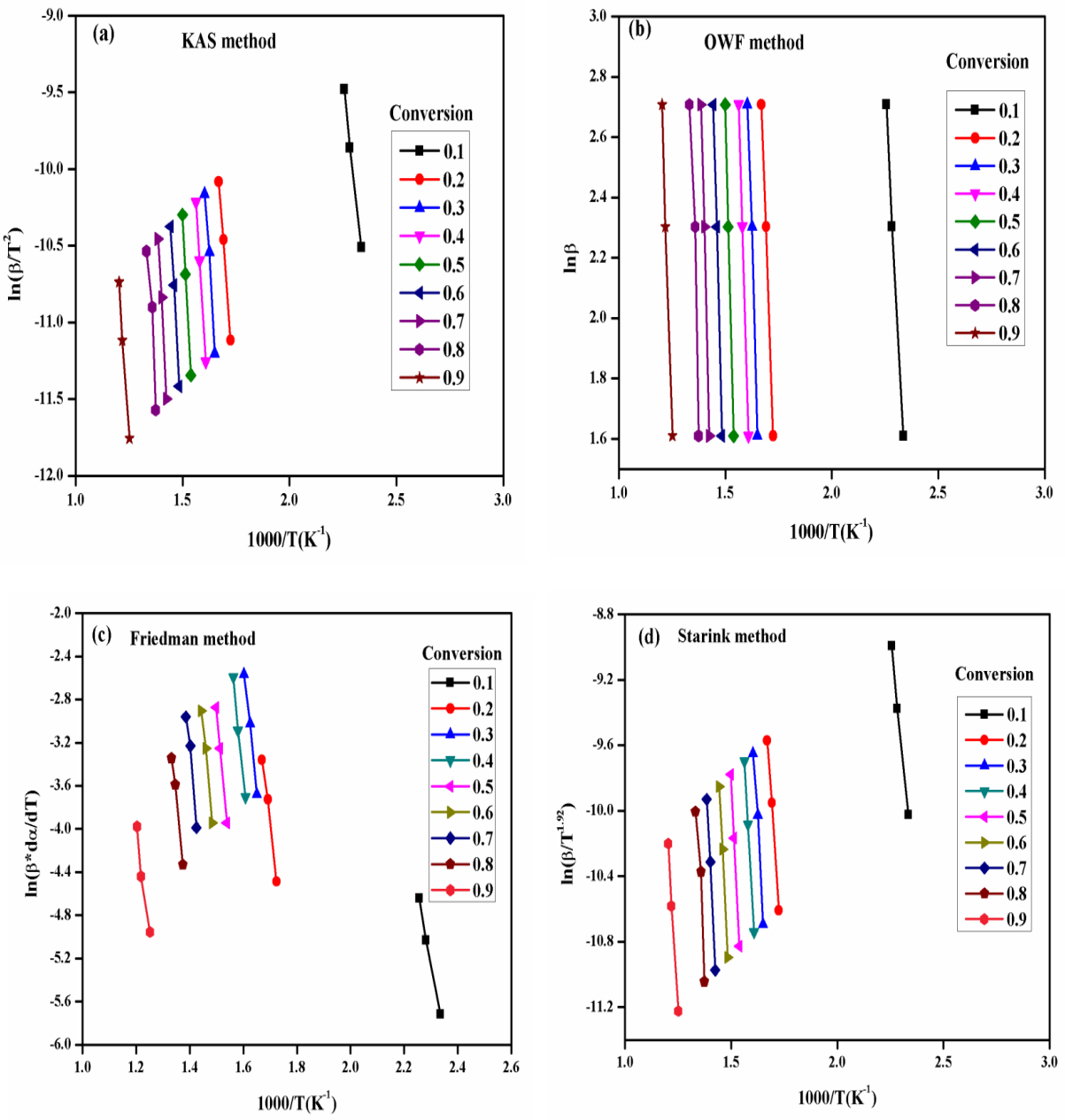

Figure 4.5 Kinetic plots for TAN-250 using (a) KAS, (b) OWF, (c) Friedman, and (d) Starink models.

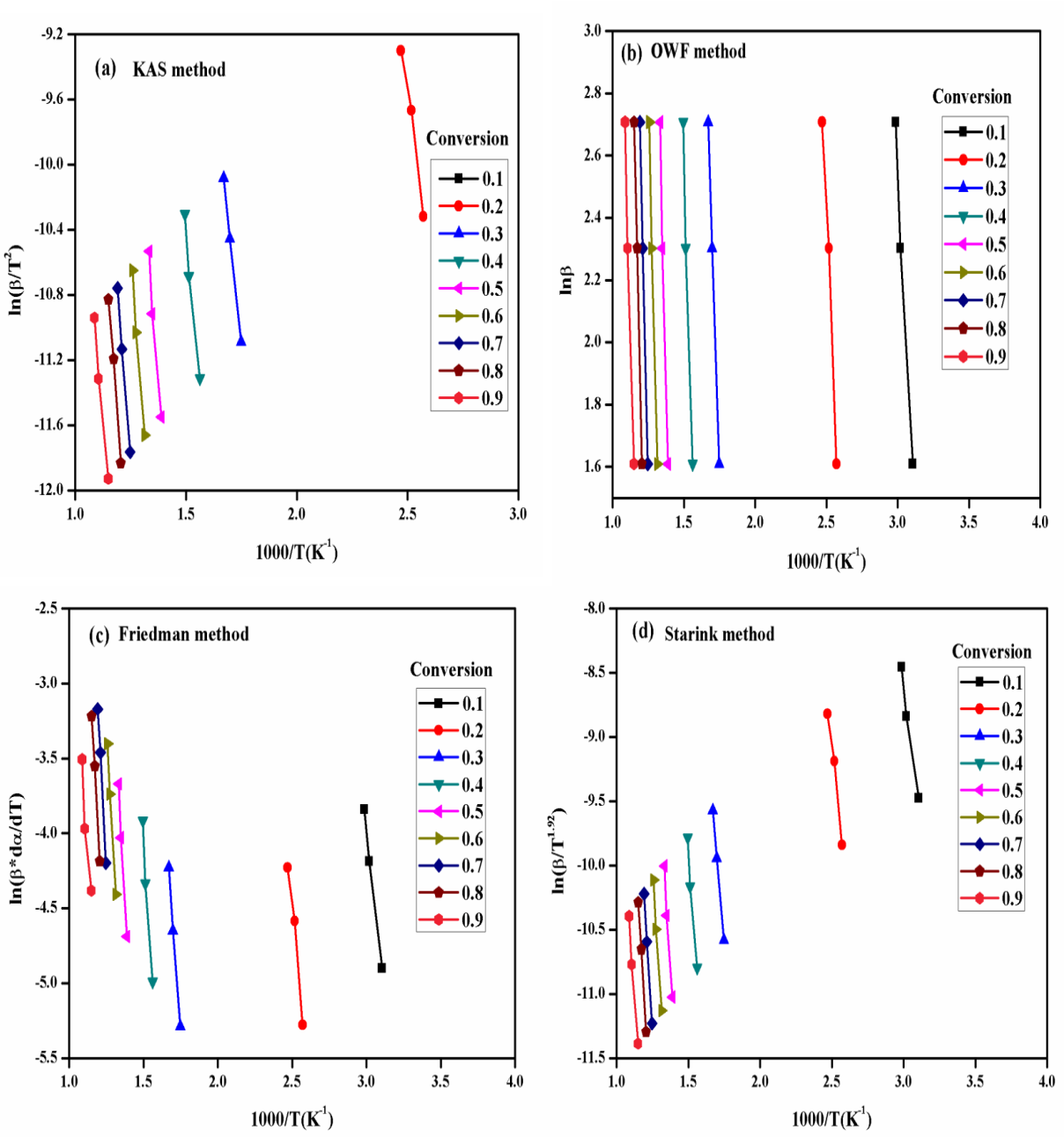

Figure 4.6 Kinetic plots for TAN-280 using (a) KAS, (b) OWF, (c) Friedman, and (d) Starink models.

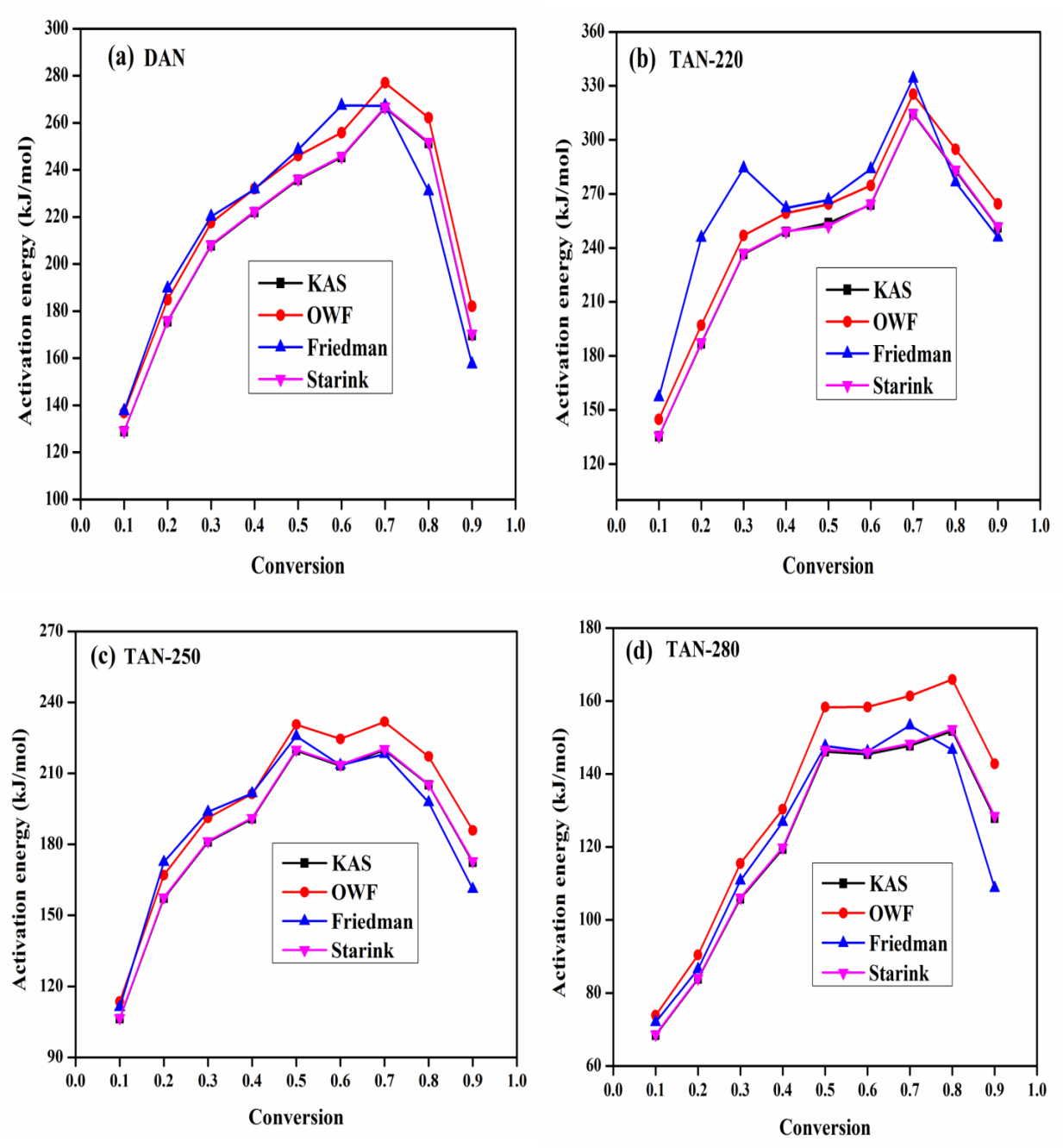

Figure 4.7 Variation of activation energy with conversion using different models: (a) DAN, (b) TAN-220 (c) TAN-250, and (d) TAN-280.

Table 4.3 The activation energy of DAN and torrefied biomass at different level of conversion using KAS, OWF, Friedman and Starink methods

Conversion	KAS method		OWF method		Friedman method		Starink method	
	E (kJ/mol)	R^2	E (kJ/mol)	R^2	E (kJ/mol)	R^2	E (kJ/mol)	R^2
DAN								
0.1	128.89	0.9966	136.84	0.9970	137.67	0.9993	129.21	0.9966
0.2	175.68	0.9900	184.84	0.9910	189.74	0.9873	176.04	0.9901
0.3	207.89	0.9806	217.52	0.9823	220.22	0.9810	208.29	0.9807
0.4	222.09	0.9804	232.03	0.9832	231.85	0.9926	222.49	0.9809
0.5	235.78	0.9992	246.05	0.9992	248.57	0.9992	236.20	0.9992
0.6	245.41	0.9970	255.83	0.9972	267.41	0.9981	245.82	0.9970
0.7	266.40	0.9929	276.98	0.9934	267.21	0.9656	266.82	0.9929
0.8	251.46	0.9882	262.18	0.9891	230.97	0.9792	251.88	0.9882
0.9	169.81	0.9853	182.01	0.9873	157.45	0.9729	170.30	09854
Average	**211.49**		**221.58**		**216.78**		**211.89**	
TAN-220								
0.1	135.29	0.9760	144.77	0.9789	157.20	0.9865	135.66	0.9761
0.2	186.95	0.9893	197.05	0.9904	245.77	0.9910	187.35	0.9894
0.3	236.64	0.9873	246.90	0.9883	284.35	0.9979	237.04	0.9874
0.4	248.88	0.9991	259.28	0.9920	262.14	0.9990	249.30	0.9991
0.5	253.79	0.9991	264.27	0.9992	266.64	0.9996	252.20	0.9991
0.6	264.06	0.9969	274.70	0.9971	283.84	0.9892	264.48	0.9969
0.7	314.44	0.9768	325.41	0.9783	334.18	0.9497	314.88	0.9769
0.8	282.87	0.9935	294.80	0.9940	276.53	0.9941	283.34	0.9936
0.9	251.34	0.9878	264.37	0.9889	245.85	0.9856	251.85	0.9878
Average	**241.58**		**252.39**		**261.83**		**241.78**	
TAN-250								
0.1	106.37	0.9973	113.61	0.9976	111.15	0.9985	106.66	0.9973

0.2	157.23	0.9975	167.03	0.9976	172.55	0.9904	157.62	0.9973
0.3	180.94	0.9783	191.17	0.9806	193.80	0.9918	181.35	0.9998
0.4	190.84	0.9998	201.33	0.9998	201.57	0.9949	191.26	0.9998
0.5	219.65	0.9930	230.60	0.9993	225.79	0.9999	220.09	0.9993
0.6	213.20	0.9972	224.56	0.9975	213.46	0.9919	213.66	0.9972
0.7	219.84	0.9923	231.76	0.9931	218.15	0.9596	220.32	0.9924
0.8	205.14	0.9915	217.12	0.9869	197.77	0.9899	205.32	0.9853
0.9	172.38	0.9939	185.91	0.9947	161.16	0.9636	172.92	0.9940
Average	**185.06**		**198.89**		**188.37**		**185.46**	
TAN-280								
0.1	68.42	0.9874	73.87	0.9891	72.00	0.9968	68.64	0.9874
0.2	83.81	0.9846	90.41	0.9868	86.54	0.9784	84.07	0.9847
0.3	105.77	0.9993	115.49	0.9994	110.80	0.9966	106.16	0.9993
0.4	119.48	0.9818	130.33	0.9846	126.83	0.9779	119.91	0.9819
0.5	146.14	0.9797	158.34	0.9824	147.71	0.9869	146.62	0.9796
0.6	145.44	0.9875	158.35	0.9893	146.17	0.9958	145.96	0.9876
0.7	147.74	0.9994	161.38	0.9995	153.28	0.9947	148.29	0.9994
0.8	151.78	0.9941	165.89	0.9951	146.64	0.9904	152.34	0.9942
0.9	127.93	0.9886	142.78	0.9907	108.73	0.9243	128.52	0.9887
Average	**121.83**		**132.98**		**122.07**		**122.27**	

4.3.4 Prediction of reaction mechanism (Criado analysis)

Criado analysis was employed to investigate the reaction mechanism during pyrolysis of DAN and torrefied biomass (TAN-220, TAN-250, and TAN-280) at a different level of conversion at a heating rate of 10 K/min. The standard kinetic models selected are

mentioned in Table 4.1. The master plots for DAN and torrefied biomass is shown in Fig. 4.8 (a-d) at conversion from 0.1 to 0.9.

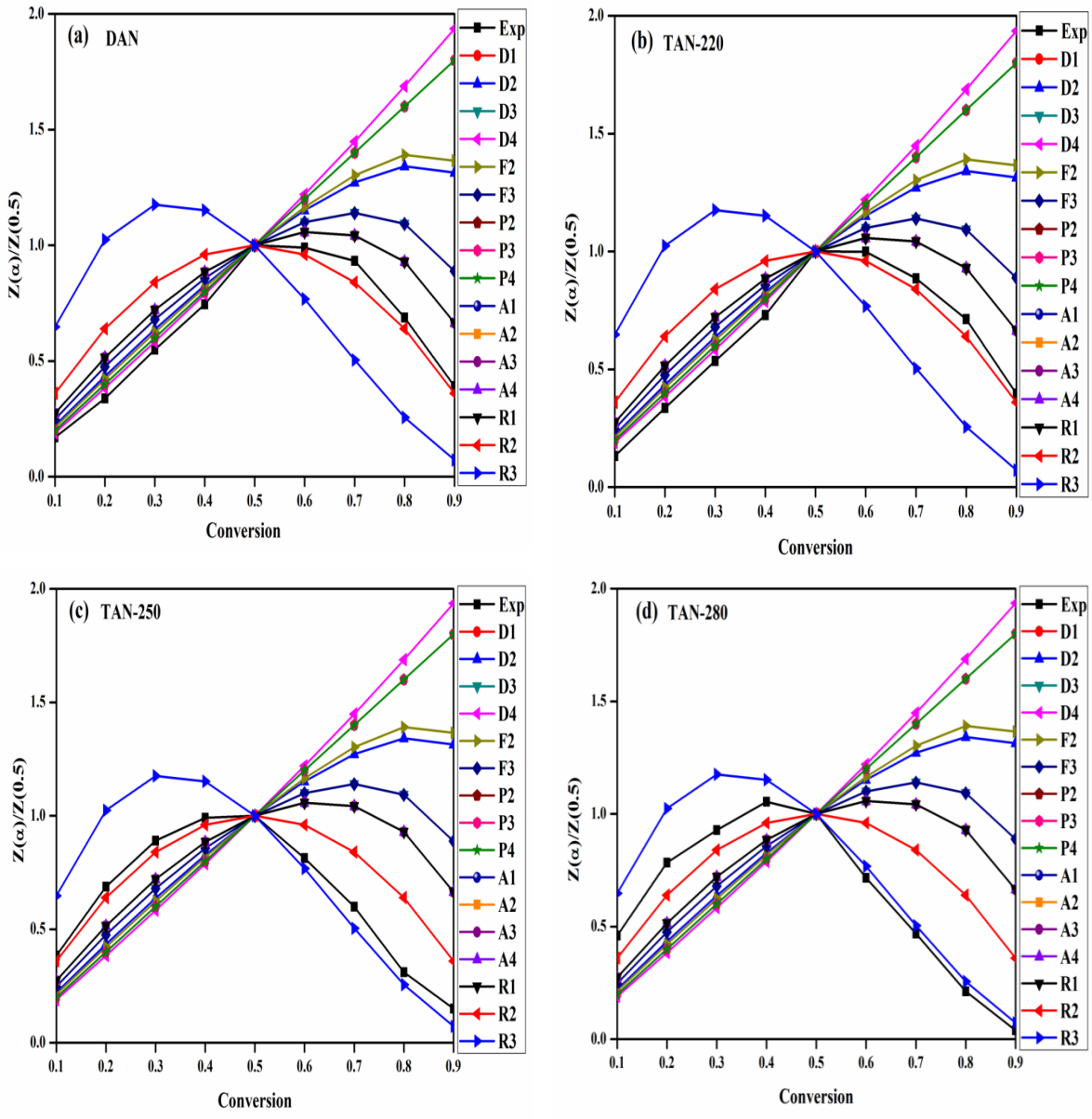

Figure 4.8 Theoretical and experimental plots for prediction of solid state reaction mechanism using Criado method (Z-master plot): (a) DAN, (b) TAN-220 (c) TAN-250, and (d) TAN-280.

4.3.4.1 Reaction mechanism at lower conversion ($\alpha < 0.5$)

Table 4.4 represents the decomposition mechanism followed by DAN and torrefied biomass (TAN-220, TAN-250, and TAN-280). For DAN and torrefied biomass (TAN-220) at conversion less than 0.5, the closest match with the theoretical curve is associated with D1, D2, D3 and D4 mechanism which corresponds to one dimensional diffusion model, two-dimensional diffusion (Valensi model), three-dimensional diffusion (Jander model) and three-dimensional diffusion (Ginstlinge-Brounshtein model), respectively. Whereas, torrefied biomass (TAN-250) follows the R2 model which corresponds to 2^{nd} order random nucleation having two nucleus on individual particle (R2) and torrefied biomass (TAN-280), followed the R2 and R3 model, which corresponds to 2^{nd} order random nucleation having two nucleus on individual particle and 3^{rd} order random nucleation having three nucleus on individual particle (R3), respectively, for the conversion less than 0.5. In case of DAN and torrefied biomass (TAN-220), the dominance of diffusion model may be due to higher volatile content. However, in case of torrefied biomass (TAN-250 and TAN-280), the volatile matter is already released in the course of torrefaction. Accordingly, random nucleation models become prominent. These results are in good agreement with the published results obtained by Doddapaneni et al. (Doddapaneni et al., 2016), Mishra et al. (Mishra et al., 2015), Poletto et al. (Poletto et al., 2012), and Vlaev et al. (Vlaev et al., 2003). Diffusion models are associated with the diffusion of gaseous products from the reactant samples. As the conversion increases, the thickness of the product layer around the sample increases. This layer around the sample can hinder the transfer of heat from the external source. Accordingly, the decomposition of the sample will be affected. Therefore, diffusion becomes the rate-determining step during the pyrolysis process at low conversion.

4.3.4.2 Reaction mechanism at higher conversion ($\alpha > 0.5$)

For higher degree of conversion (from 0.5 to 0.9), the reaction mechanism was followed by DAN and TAN are presented in Table 4.4. For DAN at conversion greater than 0.5, the closest match with the theoretical curve is associated with R2, which corresponds to 2nd order random nucleation having two nuclei on individual particle and Avrami-Erofeev models (A1, A2, A3, and A4) which is associated with nucleation and growth. Whereas, torrefied biomass (TAN-220) follows the R2 model which corresponds to 2nd order random nucleation having two nuclei on individual particle (R2) and torrefied biomass (TAN-250 and TAN-280) both followed R3 model, which corresponds to 3rd order random nucleation having three nuclei on individual particle (R3). During the decomposition process, higher conversion was achieved at relatively higher temperature. At higher temperature, cleavage of some ordered cellulose may take place which gets converted into chain of lower molecular mass. This chain of lower molecular mass might act as a site for random nucleation growth and degradation reaction.

Table 4.4 Predicted models for DAN and torrefied biomass (TAN-220, TAN-250, and TAN-280)

Biomass	**Solid state process**	
	Conversion < 0.5	**Conversion > 0.5**
DAN	Diffusion models (D1, D2, D3 and D4) D1 $f(\alpha) = 2(1-\alpha)\,[-\ln(1-\alpha)]^{1/2}$ $g(\alpha) = [-\ln(1-\alpha)]^{1/2}$ D2 $f(\alpha) = [-\ln(1-\alpha)]^{-1}$ $g(\alpha) = (1-\alpha)\ln(1-\alpha) + \alpha$ D3 $f(\alpha) = \frac{3}{2}(1-\alpha)^{2/3}\,[1-(1-\alpha)^{1/3}]^{-1}$ $g(\alpha) = [1-(1-\alpha)^{1/3}]^2$ D4 $f(\alpha) = \frac{3}{2}[(1-\alpha)^{1/3}-1]^{-1}$	2nd order random nucleation having two nucleus on individual particle (R2) R2 $f(\alpha) = (1-\alpha)^2$ $g(\alpha) = (1-\alpha)^{-1} - 1$ Avrami-Erofeev models (A1, A2, A3 and A4) A1 $f(\alpha) = \frac{1}{2}(1-\alpha)\,[-\ln(1-\alpha)]^{1/3}$ $g(\alpha) = [-\ln(1-\alpha)]^{2/3}$ A2 $f(\alpha) = 2(1-\alpha)\,[-\ln(1-\alpha)]^{1/2}$ $g(\alpha) = [-\ln(1-\alpha)]^{1/2}$

	$g(\alpha) = 1-\frac{2}{3}\alpha - (1-\alpha)^{2/3}$	A3 $f(\alpha) = 3(1-\alpha)\,[-\ln(1-\alpha)]^{2/3}$ $g(\alpha) = [-\ln(1-\alpha)]^{1/3}$ A4 $f(\alpha) = 4(1-\alpha)\,[-\ln(1-\alpha)]^{3/4}$ $g(\alpha) = [-\ln(1-\alpha)]^{1/4}$
TAN-220	Diffusion models (D1, D2, D3 and D4) D1 $f(\alpha) = 2(1-\alpha)\,[-\ln(1-\alpha)]^{1/2}$ $g(\alpha) = [-\ln(1-\alpha)]^{1/2}$ D2 $f(\alpha) = [-\ln(1-\alpha)]^{-1}$ $g(\alpha) = (1-\alpha)\ln(1-\alpha) + \alpha$ D3 $f(\alpha) = \frac{3}{2}(1-\alpha)^{2/3}\,[1-(1-\alpha)^{1/3}]^{-1}$ $g(\alpha) = [1-(1-\alpha)^{1/3}]^2$ D4 $f(\alpha) = \frac{3}{2}[(1-\alpha)^{1/3}-1]^{-1}$ $g(\alpha) = 1-\frac{2}{3}\alpha - (1-\alpha)^{2/3}$	2nd order random nucleation having two nucleus on individual particle (R2) R2 $f(\alpha) = (1-\alpha)^2$ $g(\alpha) = (1-\alpha)^{-1} - 1$
TAN-250	2nd order random nucleation having two nucleus on individual particle (R2) $f(\alpha) = (1-\alpha)^2$ $g(\alpha) = (1-\alpha)^{-1} - 1$	3rd order random nucleation having three nucleus on individual particle (R3) $f(\alpha) = (1-\alpha)^3$ $g(\alpha) = \frac{1}{2}[(1-\alpha)^{-2} - 1]$
TAN-280	2nd order random nucleation having two nucleus on individual particle (R2) R2 $f(\alpha) = (1-\alpha)^2$ $g(\alpha) = (1-\alpha)^{-1} - 1$ 3rd order random nucleation having three nucleus on individual particle (R3) R3 $f(\alpha) = (1-\alpha)^3$ $g(\alpha) = \frac{1}{2}[(1-\alpha)^{-2} - 1]$	3rd order random nucleation having three nucleus on individual particle (R3) $f(\alpha) = (1-\alpha)^3$ $g(\alpha) = \frac{1}{2}[(1-\alpha)^{-2} - 1]$

4.3.5 Thermodynamic parameters

The thermodynamic parameters were calculated by using Eqs. (4.20-4.23) based on apparent activation energy obtained from the KAS method at a heating rate of 10 K/min and corresponding values are presented in Table 4.5. Furthermore, the low value of heating rate was selected to avoid the effect of interaction between the constituents, which shows the pronounced effect at a higher heating rate (Yuan et al., 2017). The values of pre-

exponential factor for DAN and torrefied biomass (TAN-220, TAN-250, and TAN-280) at different conversion, obtained using KAS method at a heating rate of 10 K/min ranges from 10^{10} to 10^{18}, 10^{10} to 10^{25}, 10^{8} to 10^{18} and 10^{3} to 10^{9}, respectively. Pre-exponential factor depicts the nature of the complex associated with the reaction. The low value of pre-exponential factor signifies the closed complex whereas high value signifies the simple complex (Kaur et al., 2018; Yuan et al., 2017). Turmanova et al. (Turmanova et al., 2008) investigated that the value of empirical pre-exponential factor for first-order reaction generally varies from 10^{4} to 10^{18} s^{-1}. The variation in pre-exponential factor may be due to the complex nature of biomass and also due to complex thermal degradation of biomass. It was also noted that the value of pre-exponential factor is in line with the value of activation energy. At particular conversion, higher pre-exponential factor was noted at higher value of activation energy.

The Enthalpy is a thermodynamic property which signifies the total heat content of a system. In case of biomass pyrolysis, it represents the total amount of heat taken by the biomass for its conversion into different products like bio-char, bio-oil, and gases (Daugaard & Brown, 2003). The change in enthalpy with different level of conversion calculated from KAS method at 10 K/min is given in Table 4.5. The enthalpy for DAN and torrefied biomass (TAN-220, TAN-250, and TAN-280) varies from 124.97-261.18, 130.60-309.04, 102.72-214.14, and 65.66-144.69 kJ/mol, respectively. It was noticed that at each level of conversion, the difference of energy between the activation energy and enthalpy for DAN and torrefied biomass (TAN-220, TAN-250, and TAN-280) was ~2-6, ~5-6, ~4-7, and ~3-7 kJ/mol. This difference is attributed to the difference between activated complex formed during the decomposition and initial, DAN and TAN. Mehmood

et al. (Mehmood et al., 2017) illustrated that difference of activation energy and enthalpy suggested that product formation can be achieved by providing 2-6, 5-6, 4-7, and 3-7 kJ/mol of energy in case of DAN and TAN, respectively. Vlaev et al. and Loy et al. (Loy et al., 2018; Vlaev et al., 2007) illustrated that lower difference between the activation energy and enthalpy favors the formation of an activated complex which finally leads to bioenergy production through pyrolysis.

Gibbs free energy (ΔG) indicates the total increase in energy of a system for the formation of the activated complex (Kaur et al., 2018; Turmanova et al., 2008). The change in ΔG at each conversion value calculated using KAS method at 10 K/min is given in Table 4.5. The ΔG for DAN and torrefied biomass (TAN-220, TAN-250, and TAN-280) varies from 164.33-199.59, 162.78-163.47, 158.71-162.48, and 211.20-216.51 kJ/mol, respectively. It can confer that, DAN, the variation in ΔG is higher; however, for TAN the value of ΔG, remains almost constant for all value of conversion from 0.1 to 0.9. A positive value of ΔG for DAN and torrefied biomass (TAN-220, TAN-250, and TAN-280) reveals the unfavorable reactions that consume a considerable amount of energy to occur (Mallick et al., 2018). Similar results of ΔG for different biomass have been reported by Xu et al. (Xu & Chen, 2013) for rice straw, Ahmad et al. (Ahmad et al., 2017) for para grass, and Huang et al. (Huang et al., 2018) for sewage sludge.

The entropy, being a state function, represents the degree of disorder or randomness associated with the reaction system. The change in entropy (ΔS) at different value of conversion is given in Table 4.5. It was found that ΔS for DAN and torrefied biomass (TAN-220 and TAN-250) has both positive and negative values varies in the range of −44.96 to 96.42, −51.82 to 230.24, and −13.03 to 88.81 J/mol.K, respectively. The larger

value of ΔS indicates that biomass sample is away from the thermodynamic equilibrium, while smaller value of ΔS means that biomass sample is acquiring a new state which is approaching it to state of thermodynamic equilibrium. However, TAN-280 has only negative ΔS in the range of −2.20 to −0.43 J/mol.K. The negative value of entropy is the result of disordered nature of product formed through bond dissociation. The low value of entropy also suggests that material has just passed through some physical and chemical changes, which bring the material to the state of thermodynamic equilibrium during the pyrolysis process (Kaur et al., 2018; Yuan et al., 2017).

Table 4.5 Thermodynamic parameters for pyrolysis of DAN and torrefied biomass at a heating rate of 10 K/min

Conversion	A (s^{-1})	ΔH (kJ/mol)	ΔG (kJ/mol)	ΔS (J/mol.K)
DAN				
0.1	1.42×10^{10}	124.97	164.33	−62.13
0.2	1.33×10^{11}	171.18	199.54	−44.96
0.3	6.88×10^{13}	203.17	199.36	5.45
0.4	1.07×10^{15}	217.22	199.33	27.52
0.5	1.51×10^{16}	230.73	199.32	48.72
0.6	9.69×10^{16}	243.22	199.32	63.71
0.7	5.53×10^{18}	261.20	199.35	96.42
0.8	3.11×10^{17}	246.18	199.32	72.93
0.9	4.23×10^{10}	163.83	199.59	−56.56
TAN-220				
0.1	5.61×10^{10}	130.60	163.47	−51.82
0.2	1.39×10^{15}	181.97	162.93	30.01
0.3	2.18×10^{19}	231.59	162.78	108.48
0.4	2.33×10^{20}	243.77	162.79	127.67

0.5	6.04×10^{20}	248.63	162.79	135.33
0.6	4.40×10^{21}	258.84	162.81	151.39
0.7	7.39×10^{25}	309.04	163.00	230.24
0.8	1.67×10^{23}	277.00	162.86	179.95
0.9	3.76×10^{20}	244.91	162.78	129.48
TAN-250				
0.1	2.62×10^{8}	102.72	162.48	−95.73
0.2	6.99×10^{12}	152.31	160.45	−13.03
0.3	7.76×10^{14}	175.82	159.72	25.79
0.4	5.51×10^{15}	185.57	159.44	41.86
0.5	1.64×10^{18}	214.15	158.71	88.81
0.6	4.58×10^{17}	207.50	158.87	77.91
0.7	1.70×10^{18}	213.91	158.71	88.43
0.8	9.32×10^{16}	198.98	159.07	63.94
0.9	1.42×10^{14}	165.55	159.97	8.93
TAN-280				
0.1	3.70×10^{3}	65.66	216.51	−2.20
0.2	4.57×10^{4}	80.50	215.16	−1.60
0.3	1.56×10^{6}	100.87	213.61	−1.06
0.4	1.38×10^{7}	113.98	212.80	−0.82
0.5	9.21×10^{8}	139.96	211.45	−0.48
0.6	8.26×10^{8}	138.91	211.49	−0.49
0.7	1.18×10^{9}	140.87	211.38	−0.47
0.8	2.23×10^{9}	144.69	211.20	−0.43
0.9	5.24×10^{7}	120.40	212.34	−0.71

4.4 Conclusions

Torrefaction of *Acacia nilotica* was performed in a fixed bed reactor at three different temperatures 220, 250 and 280 ℃, keeping retention time and heating rate constant. The TGA of DAN and TAN was performed at three different heating rate viz. 5, 10 and 15 K/min. Based on the result of TGA analysis, kinetic, thermodynamic parameters and reaction mechanism during pyrolysis of DAN and TAN were investigated. Compositional analysis showed that at lower temperature during torrefaction, the relative cellulose content in the torrefied biomass (TAN-220) is higher than the DAN, while, it goes on decreasing on further increase in temperature. The higher cellulose content attributed to higher activation energy of TAN-220 than DAN. The average activation energy of torrefied biomass obtained at 280 ℃ (TAN-280) is 42.39% lower than the DAN. Slight difference between activation energy and enthalpy favors the formation of activated complex. Accordingly, bio-energy generation through pyrolysis can be positively attained. It was noticed that at lower conversion value ($\alpha \leq 0.5$) the diffusion mechanism was rate determining for DAN and TAN-220, however, for TAN-250 and TAN-280, the 2nd order random nucleation model is dominant for rate determination. At higher conversion ($\alpha \geq 0.5$), DAN and TAN-220 follow the 2nd order random nucleation and Avrami-Erofeev models, while, in case of TAN-250 and TAN-280, 3rd order random nucleation is dominant. Finally, it can be concluded that the behavior of DAN and TAN towards thermochemical is quite different. The TAN has much improved properties than the DAN which makes it good quality solid fuel for bio-energy generation. Also, it can be blended with coal in thermal power plants.

Chapter 5

Optimization of process parameters for torrefaction of A*cacia nilotica* using response surface methodology and characteristics of torrefied biomass as upgraded fuel

General background

This chapter dealt with the optimization of process parameters for torrefaction *Acacia nilotica* (TAN) using response surface methodology. The temperature (220-280 ℃), retention time (20-60 min), and heating rate (5-15 ℃/min) were selected as independent variables and energy yield and higher heating value of TAN were selected as dependent variables. The ANOVA and regression analysis were used to study the fitness of developed model using central composite design technique. In addition, the characteristics of torrefied biomass at optimized condition were tested using TGA, FTIR, XRD, BET, and SEM analysis and compared with DAN. Moreover, the fuel characteristics like fuel ratio (FR), combustibility index (CI), volatile ignitability (VI), flow behavior through angle of repose, Hausner ratio (HR), Carr compressibility index (CCI), cohesion coefficient (C), moisture sorption ability and densities (bulk, tapped and particle) of TAN at optimized condition and DAN were also compared.